ЖЭТФ, 2014, том 145, вып. 2, стр. 272–278

FIRST-PRINCIPLE STUDY OF THE STRUCTURAL, ELECTRONIC, AND THERMODYNAMIC PROPERTIES OF CUPROUS OXIDE UNDER PRESSURE

M. Zemzemi [a]*, ***N. Elghoul*** [a], ***K. Khirouni*** [a], ***S. Alaya*** [a,b]

[a] *Laboratoire de Physique des Matériaux et des Nanomatériaux appliquée à l'Environnement, Université de Gabès, Faculté des Sciences de Gabès, Citè Erriadh Zrig 6072, Gabès, Tunisie*

[b] *King Faisal University, College of Science, Physics Department 31982, Hofuf, Saudi Arabia*

Received March 18, 2013

Cuprous oxide is selected as a promising material for photovoltaic applications. Density functional theory is used to study the structural, electronic, and thermodynamic properties of cuprous oxide by using the local density approximation and generalized-gradient approximation. The effect of pressure on the structural and electronic properties of Cu_2O is investigated. This study confirms and characterizes the existence of new phases. Hexagonal and tetragonal phases are not completely indentified. We focus on the phase transition of the cuprous oxide under hydrostatic pressure to tetragonal and hexagonal (CdI_2) structures. Variation of enthalpy with pressure is used to calculate the pressure of the phase transition.

DOI: 10.7868/S0044451014020084

1. INTRODUCTION

Metal oxides are widely used in various applications such as electronic components, building materials and refractories in drastic conditions of pressure and/or temperature. Studies of metal oxides are thus of great importance for obtaining a better understanding of corrosion of metals, heterogeneous catalysis, gas sensors, and transparent conductive oxides. The cuprous oxide (Cu_2O) was the first substance known to behave as a semiconductor, together with selenium [1]. Most of the semiconductor theories were developed using the data on Cu_2O. This oxide remains an attractive alternative material to silicon and other semiconductors, being favored at present for many applications due to its many advantages. It is nontoxic, its starting material (which is copper) is very abundant, and its production process is simple [2]. The most important methods for the production of Cu_2O are thermal oxidation, electrodeposition, and sputtering technique [3–5].

Cuprous oxide is a potential material for fabrication of low-cost solar cells [6, 7]. The first real solar cell with Cu_2O was fabricated in the late 1920s. But at that time, and until the first space explorations, the energy production from the sun by photovoltaic effect was just a curiosity. High-efficiency Cu_2O-based solar cells require a good understanding of the crystallinity of this oxide and a judicious choice of the structural orientation. Cu_2O is a p-type semiconductor; it crystallizes in the cubic structure ($Pn-3m$) and has a direct band gap of about 2 eV [8], which is suitable for photovoltaic conversion [9, 10].

Cuprous oxide has been the subject of numerous theoretical and experimental studies, but still its electronic and atomic structures continue to puzzle the researchers. New applications of Cu_2O in nanoelectronics, spintronics, superconductivity, and photovoltaics are emerging [11, 12]. A better understanding of the atomic structure and electronic levels of cuprous oxide may be useful for predicting and controlling the phase transition under hydrostatic pressure, which will in turn allow a better understanding of the growth mechanism. Metal oxides present many polymorphs. The stability and mechanism of phase transitions represent an active field of investigation to discover a new stable phase or improve an existent one [13]. In ambient conditions, Cu_2O stabilizes in a simple cubic Bra-

*E-mail: mzemzemi@gmail.com

vais lattice, with the space group $Pn-3m(223)$ [14]. Under high pressure, the cubic phase has a number of low-pressure phases. These phase transitions have been studied both theoretically and experimentally [15, 16]. Experimental studies have shown that cuprous oxide grows preferntially along the (111) direction [17, 18]. Atomic stacking along this direction coincides well with the hexagonal structure [19].

The present work is focused on clarifying some fundamental aspects of Cu_2O that can be important for both device fabrication and a better understanding of the physical phenomena observed in Cu_2O. The aim of this work is to characterize hexagonal and tetragonal structure of cuprous oxide. We focus on the effect of pressure in the structural and electronic properties of Cu_2O polymorphs. A relation is established between the electronic structure and the phase transition mechanism in Cu_2O.

2. COMPUTATIONAL DETAILS

Theoretical calculations are performed in the framework of the density functional theory (DFT) [20, 21] using pseudopotentials and a plane-wave basis implemented in the ABINIT package [22]. This package is available under a free software licence and allows computing a large set of useful properties for solid state studies [23]. The valence electron wavefunctions are expanded in plane waves with the kinetic energy cutoff E_{cut} equal to 50 Hartree. The pseudopotentials are generated with the respective $3d^{10}4s^1$ and $2s^22p^4$ atomic configurations of copper and oxygen. Norm-conserving pseudopotentials [24] of Troullier–Martins (TM) scheme [25], generated from the Fritz-Haber-Institute package [26], are used. The exchange-correlation terms were depicted, first, with the local density approximation of Ceperly and Adler [27] by the parameterization of Perdew and Zunger [28]; on the other hand, we used the generalized-gradient approximation (GGA) proposed by Perdew, Burke, and Ernzerhof (PBE) [29]. For the Brillouin zone sampling, the $8\times8\times8$ k-points distributed on a shifted Monkhorst–Pack grid was used [30]. The numerical results given below correspond to zero temperature. A judicious choice of the E_{cut} value and the k-point number is very important because if we increase these numbers, the CPU time and memory space also increase.

3. RESULTS AND DISCUSSION

Under ambient conditions, Cu_2O crystallizes in a simple cubic structure, which belongs to the space group $Pn-3m$. It can be described as a cubic unit cell where oxygen atoms are in the corners with a tetrahedral unit of Cu_4O at the center (Fig. 1 *a*). In the lattice, each copper atom coordinates with two oxygen atoms and each oxygen atom is surrounded by four copper atoms, which makes the stoichiometry 2:1. The atomic coordinates and space group of cuprous oxide are listed in Table 1. To obtain the equilibrium bulk structure, the total energy is minimized with respect to the unit cell volume. Figure 2 shows a parabolic dependence of the energy as a function of the volume. The volume corresponding to the minimum energy identifies the equilibrium lattice parameter. The lattice parameters and bulk modulus are determined by fitting a set of data points to the Murnaghan equation of state [31]. A fit of the resulting energy versus volume curve with the Murnaghan equation, shown in Fig. 2, gives the values of B_0 and its pressure derivative $B' = dB_0/dP$ for cuprous oxide. Our calculated lattice parameters, the bulk moduli B_0 and B' together with other theoretical and experimental values are listed in Table 2.

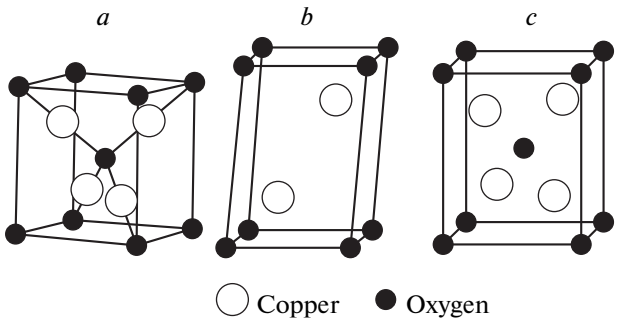

Fig. 1. (*a*) Cubic, (*b*) hexagonal CdI_2-type, and (*c*) tetragonal conventional unit cell for copper oxide

Our results are in good agreement with the published experimental and theoretical data [15, 16, 32, 33]. For cuprous oxide, the local density approximation (LDA) calculations show the well-known overbinding effect value with a lattice parameter underestimated by $-1.17\,\%$ compared to the experimental results, and GGA-PBE calculation is overestimated by $2.10\,\%$.

Under hydrostatic pressure, in the range 0–10 GPa, cuprous oxide transforms into tetragonal or hexagonal structure (Fig. 1). It was confirmed in [16] that the cubic Cu_2O becomes tetragonal under 5.7 GPa. On the other hand, as shown in [15], the oxide undergoes a phase transition toward an hexagonal structure under a pressure of 10 GPa. In this study, we have detailed the structural and electronic information of the tetragonal and hexagonal structures. We calculated and verified

Table 1. Space group and atomic positions for copper oxide in the cuprous, hexagonal, and tetragonal structures [14]

Structure	Space group	Atomic positions	
Cuprous	$Pn-3m(223)$	Cu	(1/4, 1/4, 1/4); (1/4, 3/4, 3/4)
			(3/4, 1/4, 3/4); (3/4, 3/4, 1/4)
		O	(0, 0, 0); (1/2, 1/2, 1/2)
Hexagonal (CdI_2)	$P-3m(164)$	Cu	(2/3, 1/3, 1/4); (1/3, 2/3, 1/4)
		O	(0, 0, 0)
Tetragonal	$P4_2/nnm(134)$	Cu	(1/4, 3/4, 1/4); (3/4, 1/4, 3/4)
			(3/4, 3/4, 3/4); (1/4, 1/4, 3/4)
		O	(0, 0, 0); (1/2, 1/2, 1/2)

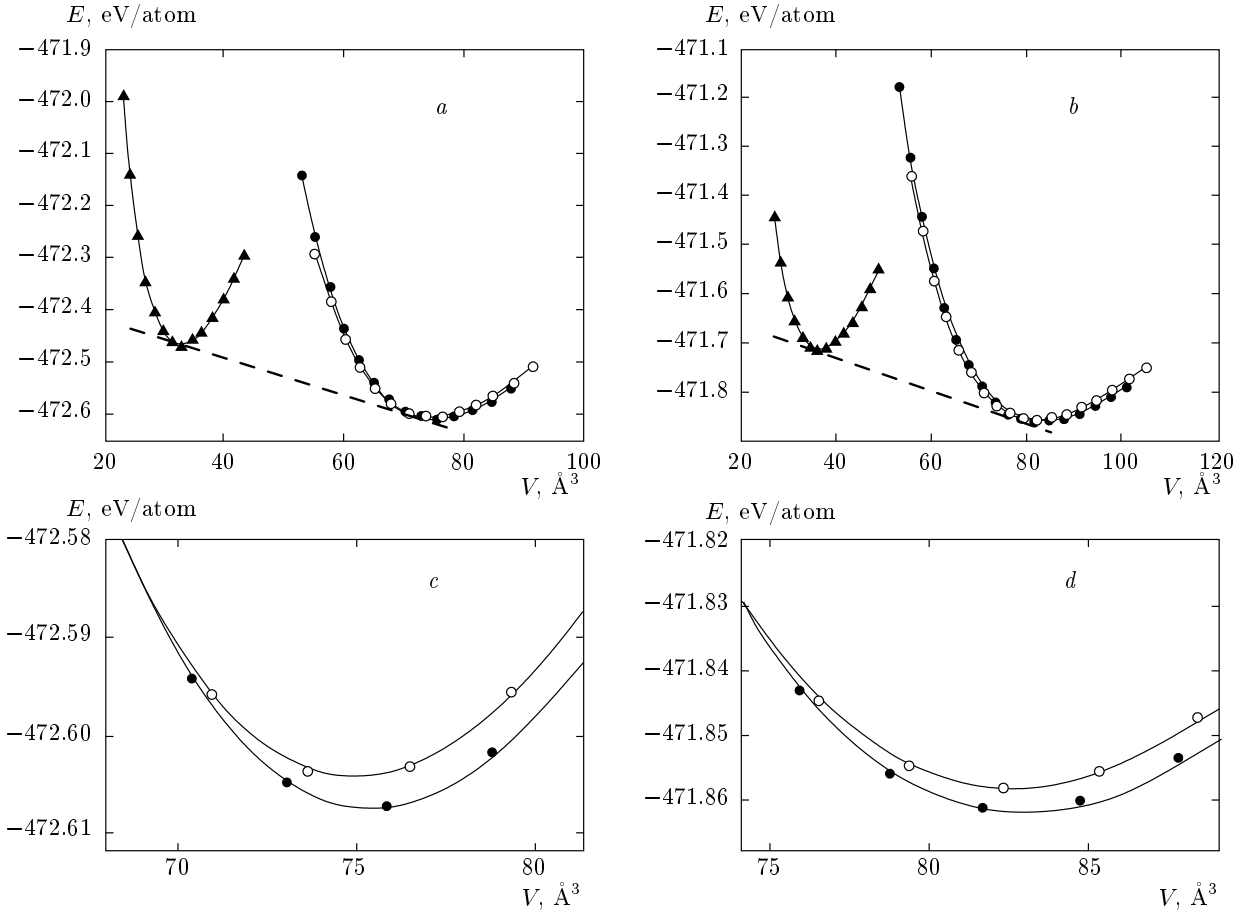

Fig. 2. Total energies as a function of the unit cell volumes for the (•) cubic, (▲) hexagonal (CdI_2), and (○) tetragonal conventional unit cell for copper oxide with the (a,c) LDA and (b,d) PBE approximation. Figures c and d are a zoom of the area showing cubic (•) and tetragonal (○) energies versus volume curves

the phase-transition pressure value. Table 1 summarizes the atomic positions and space group for the three structures. The atoms in the hexagonal and tetragonal structures are ordered in planes and form a lamellar structure. In order to look for the structural phase transition, the total energies are obtained as a function of the cell volume in the three structures.

The total energy versus volume curves calculated

Table 2. Calculated and experimental lattice parameters, bulk modulus, and pressure derivative of the bulk modulus for copper oxide in the cuprous, hexagonal, and tetragonal structures

Structure	a, Å	c, Å	B_0, GPa	B'	Reference	
Cuprous	4.22		141.14	4.23	LDA	This study
	4.36		105.58	4.15	GGA	
	4.22 [15] 4.26 [32]		141.00 [15] 136.10 [32]	– 4.67 [36]	Other calculations	
	4.27		114.10		Experiment [33]	
Hexagonal (CdI_2)	2.48	3.90	137.91	4.45	LDA	This study
	2.52	3.86	103.11	4.34	GGA	
	2.90	3.86			Experiment [34]	
Tetragonal	3.88	4.39	156.69	4.52	LDA	This study
	4.02	4.53	112.10	4.71	GGA	
	4.19	4.24			Experiment [35]	

with the LDA and GGA-PBE for the three structures and fitted by the Murnaghan equation of state are shown in Fig. 2. For the hexagonal structures, the calculated variation of the a/c ratio versus energy is not shown. The calculated values of lattice parameters, the bulk moduli B_0 and B' for tetragonal and hexagonal structures of Cu_2O under pressure, and other experimental values available in the literature are reported in Table 2. Comparison between our results and experience shows a good agreement, albeit with a small difference between the results obtained using the LDA and GGA. The plot of the total energy E per atom versus unit cell volume V with the LDA and GGA (Fig. 2*a*,*b*) shows two curves that are very close to the cubic and tetragonal structures. The difference between these two curves is clearly seen in Figs. 2*c* and 2*d*. This observation is evident because the structural transition from cubic to tetragonal is under small distortion. In Fig. 2, the dashed lines are common tangents, and the phase transition pressure is given by the slope of these lines.

The pressure at which a phase transition occurs can be deduced from the common tangent between cubic–hexagonal and tetragonal–hexagonal energy–volume curves. The pressure of the phase transition is obtained via the tangent construction using the energy versus volume plot for the two phases, i. e.,

$$P_t = -\frac{E_1 - E_2}{V_1 - V_2},$$

where P_t is the phase transition pressure, E_1 and E_2 are the respective energies at the transition for cubic and hexagonal structures, and V_1 and V_2 are the transition volume for these structures.

The same method is repeated for the cubic–tetragonal phase transition, but it is very difficult to use the common slope in this case because the two curves are very close. This method is not very accurate. However, for pressure-induced phase transitions, it is more suitable to consider the Gibbs free energy. In thermodynamics, at constant temperature and pressure, the state of a system is determined by the Gibbs free energy

$$G = E + PV - TS = H - TS,$$

where E and H denote the internal energy and enthalpy, T and S are the temperature and entropy, and P and V are the pressure and volume. We consider only the zero-temperature limit in our calculation; then the Gibbs free energy becomes equal to the enthalpy

$$H = E + PV.$$

The fit of the curves H versus P has been performed using the equation

$$G(P) = H(P) = E_0 + \frac{B_0 V_0}{B' - 1} \times \left[\left(1 + \frac{B'}{B_0} P\right)^{(B'-1)/B'} - 1\right],$$

where E_0 and V_0 are the energy and volume at equilibrium conditions, and B_0 and B' are the values of the bulk modulus and its pressure derivative at $P = 0$.

Table 3. Calculated and experimental structural transition pressures

	P_t, GPa		
	This study		
	LDA	GGA-PBE	Other results
Cubic → tetragonal	2.93	4.00	5.7 [16]
Cubic → hexagonal	6.60	8.00	7(LDA)–10(PBE) [15]
Tetragonal → hexagonal	6.81	8.25	–

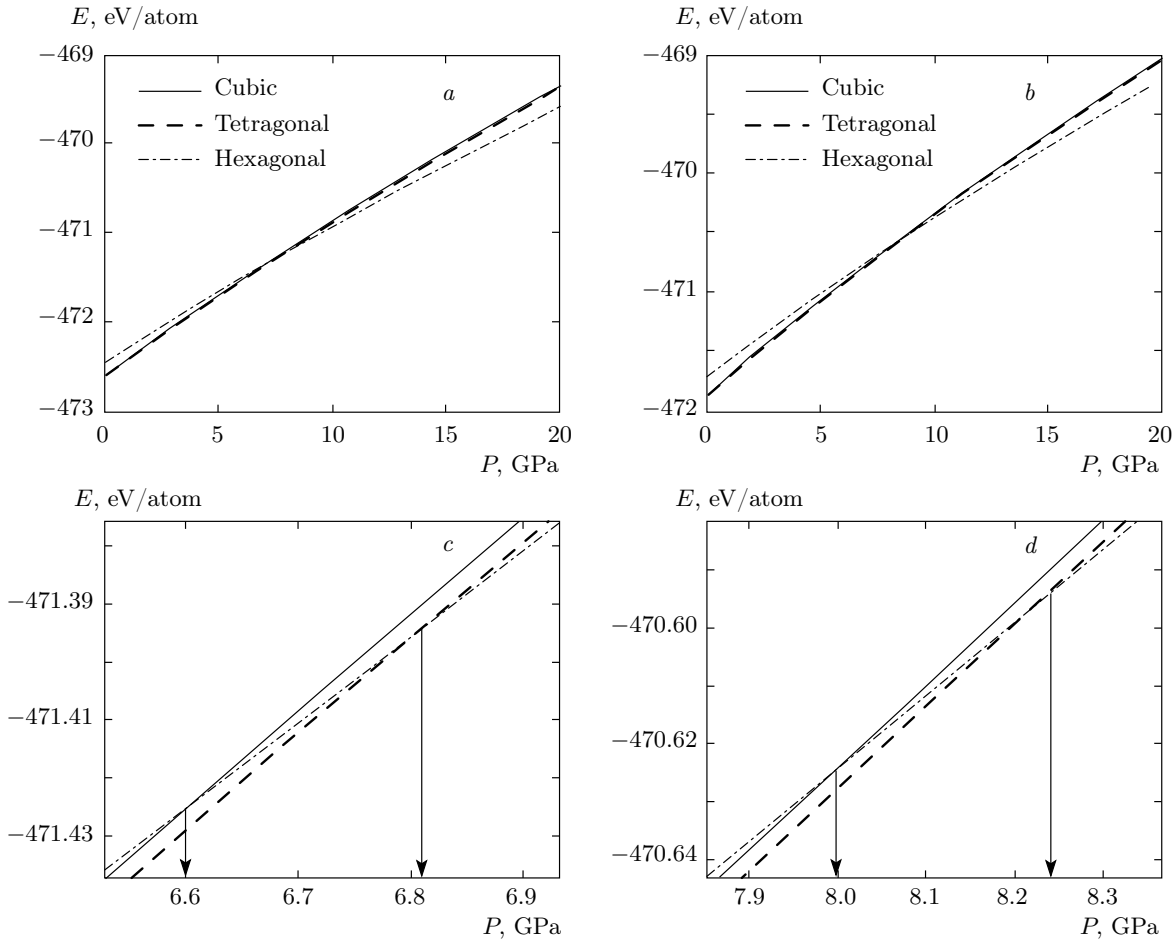

Fig. 3. Variation of enthalpy versus pressure in the cubic, hexagonal, and tetragonal copper oxide with the (a, c) LDA and (b, d) PBE approximation. Figures c and d are a zoom of the area showing intersection lines of enthalpy versus pressure

This equation of state depends on a few parameters and covers a wide range of pressures [37]. This approach relies on some knowledge or intuition of reasonable candidate crystal structures [38]. It depends on the nature of the interatomic interactions and thus provides an insight into the nature of the solid state. At the same time, it determines the values of fundamental thermodynamic parameters [39].

Generally, the results are in good agreement with experiments. The minimum enthalpy state is the thermodynamic condition of stability at zero temperature and at constant pressure. The equilibrium pressure is determined by the intersection of the two Gibbs free energy isotherms (Fig. 3). At P_t, two phases have the same enthalpy, and the transition pressure is then determined by equating the enthalpies of the two phases

of cuprous oxide. To see the possible phase transitions, Fig. 3*a*,*b* shows the calculated enthalpy curves of the cubic, tetragonal, and hexagonal cuprous oxide as a function of pressure. Figures 3*c* and 3*d* are a zoom of the area of the intersection of lines of enthalpy versus pressure. The transition pressures of Cu_2O are calculated and the results are summarized in Table 3. These values are in agreement with recent experimental and theoretical reports [15, 16].

Through this study, we find the following. The pressures calculated with both LDA and GGA-PBE are smaller than the experimental values. Hydrostatic pressure deforms the cubic structure to tetragonal at low pressure. Our PBE result (4.7 GPa) is slightly smaller than the experimental results (Table 3). Cubic–hexagonal deformation is in the vicinity of 10 GPa. Our calculation yields 8 GPa. The passage from the tetragonal to hexagonal structure is not known in the literature. This work confirms the existence of a tetragonal–hexagonal phase transition. Our study gives a value of the transition pressure with the LDA and GGA.

Figure 4 shows the band structure of copper oxide in the three different structures at the experimental lattice parameter. The maximum of the valence bands is set to the zero energy in all plots. For cuprous oxide, it is observed that the direct band gap is about 0.48 eV at the highly symmetric Γ point, which is close to the previously calculated result with the same approximations [40, 41]. The experimental value of the gap energy is 2.17 eV [42]. The underestimated band gap can be due to the choice of the exchange-correlation energy. In this study, the band gap is calculated with the LDA. Our *ab initio* calculation shows that the fundamental gap of cuprous oxide is a direct one, with the maximum of the valence band and the minimum of the conduction band occurring at the Γ point (see Fig. 4). Under pressure, the electronic structure undergoes a drastic deformation. Cuprous oxide loses its semiconductor character and we observe an overlap between valence and conduction bands. This is normal because tight bands occur as the effect of pressure.

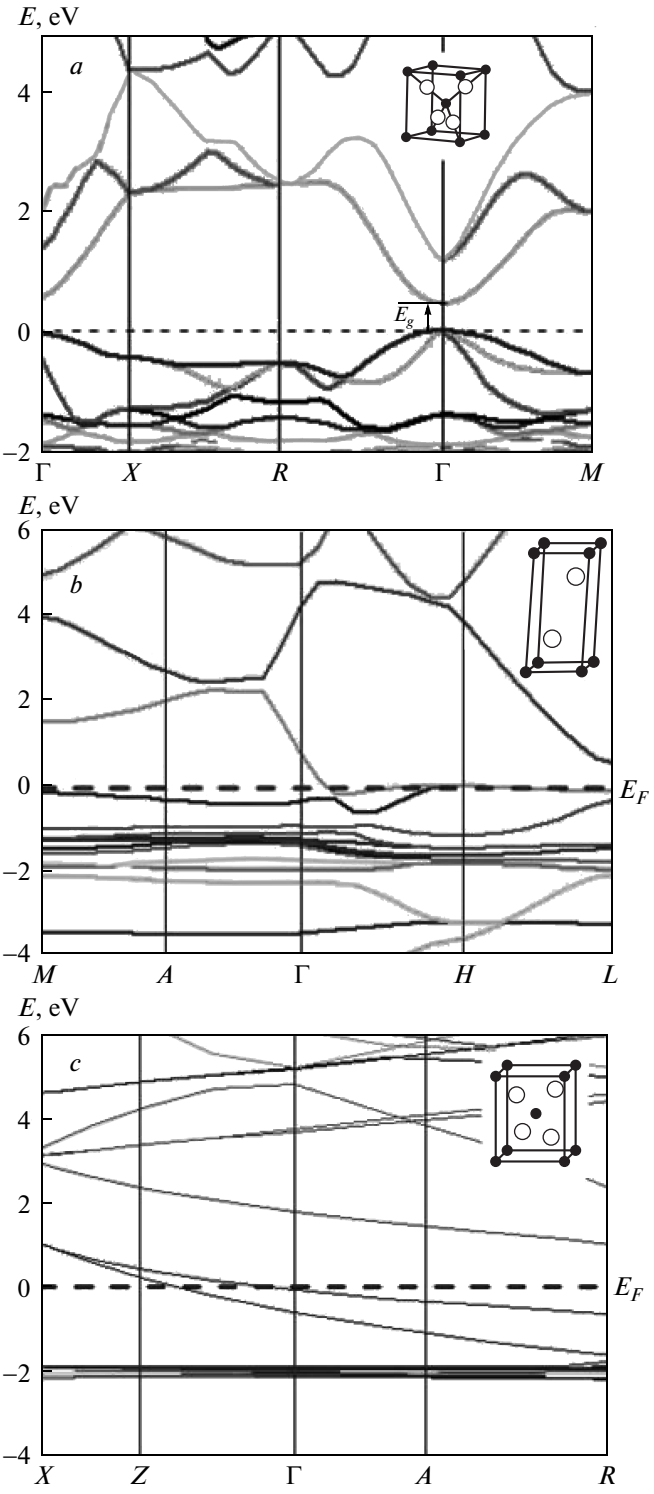

Fig. 4. Energy band diagram of copper oxide calculated for specific directions in the first Brillouin zone: (*a*) cubic, (*b*) tetragonal, and (*c*) hexagonal structures

4. CONCLUSION

A DFT study has been performed to evaluate the structural, thermodynamic, and electronic properties of Cu_2O in cubic structure and two different polymorphs under pressure. The electronic structures of the cuprous oxide and two polymorphs are reproduced. In the cubic structure, Cu_2O is shown to have a semiconductor character with the band gap underestimated because we use the LDA in our calculation. Tetrago-

nal and hexagonal structures are conductive in our approximations. In this study, we have used enthalpy versus pressure curves to calculate the transition pressure. The value of the transition pressure of the cubic to the tetragonal and hexagonal phase is calculated in very good agreement with results in the literature. These Cu_2O polymorphs have been reanalyzed with the goal to properly characterize each structure; this contribution can be used in a predictive way for manufacturing high-efficiency and more stable solar cells.

REFERENCES

1. W. H. Brattain, Rev. Mod. Phys. **23**, 203 (1951).
2. C. Leygraf, *Atmospheric Corrosion*, Wiley, New York (2000).
3. A. E. Rakhshani, A. A. Al-Jassar, and J. Varghese, Thin Solid Films **148**, 191 (1987).
4. G. P. Pollack and D. Trivich, J. Appl. Phys. **46**, 163 (1975).
5. R. P. Wijesundera, M. Hidaka, K. Koga et al., Thin Solid Films **500**, 241 (2006).
6. G. Beensh-Marchwicka, L. Krol-Stepniewska, and M. Slaby, Thin Solid Films **88**, 33 (1982).
7. Y. Zhou and J. A. Switzer, Scripta Mater. **38**, 1731 (1998).
8. J. Ghisjen, L. H. Tjeng, J. Elp, and H. Eskes, Phys. Rev. B **38**, 11322 (1988).
9. S. Nikitine, J. B. Grun, and M. Sieskind, J. Phys. Chem. Sol. **17**, 292 (1961).
10. Ch. Uihlein, D. Fröhlich, and R. Kenklies, Phys. Rev. B **23**, 2731 (1981).
11. A. Mittiga, E. Salza, F. Sarto et al., Appl. Phys. Lett. **88**, 163502 (2006).
12. T. Minami, T. Miyata, K. Ihara et al., Thin Solid Films **494**, 47 (2006).
13. F. J. Manjón and D. Errandonea, Phys. Stat. Sol. (b) **246**, 9 (2009).
14. R. W. G. Wyckoff, *Crystal Structures*, Vol. 1, Wiley, New York (1965).
15. P. Cortona and M. Mebarki, J. Phys.: Condens. Matter. **23**, 045502 (2011).
16. D. Manchon, V. V. Sinitsyn, V. P. Dmitriev et al., J. Phys.: Condens. Matter. **15**, 7227 (2003).
17. A. Onsten, M. Gothelid, and U. O. Karlsson, Surf. Sci. **603**, 257 (2009).
18. K. H. Schulz and D. F. Cox, Phys. Rev. B **43**, 1610 (1991).
19. F. Jensen, F. Besenbacher, E. Lægsgaard, and I. Stensgaard, Surf. Sci. Lett. **259**, 774 (1991).
20. P. Hohenberg and W. Kohn, Phys. Rev. **136**, 864 (1964).
21. W. Kohn and L. J. Sham, Phys. Rev. **140**, 1133 (1965).
22. X. Gonze, J.-M. Beuken, R. Caracas et al., Comput. Mater. Sci. **25**, 478 (2002) (http://www.abinit.org).
23. X. Gonze, B. Amadon, P.-M. Anglade et al., Comput. Phys. Comm. **180**, 2582 (2009).
24. W. C. Topp and J. J. Hopfield, Phys. Rev. B **7**, 1295 (1973).
25. N. Troullier and J. L. Martins, Phys. Rev. B **43**, 1993 (1991).
26. M. Fuchs and M. Scheffler, Comput. Phys. Comm. **119**, 67 (1999).
27. D. M. Ceperley and B. J. Alder, Phys. Rev. Lett. **45**, 566 (1980).
28. J. P. Perdew and A. Zunger, Phys. Rev. B **23**, 5048 (1981).
29. J. P. Perdew, K. Burke, and M. Ernzerhof, Phys. Rev. Lett. **77**, 3865 (1996).
30. H. J. Monkhorst and J. D. Pack, Phys. Rev. B **13**, 5188 (1976).
31. F. Murnaghan, Proc. Nat. Acad. Sci. USA **30**, 244 (1944).
32. F. Bruneval, Ph. D Thesis, Ecole Polytechnique, Paris (2005).
33. A. Sanson, F. Rocca, G. Dalba et al., Phys. Rev. B **73**, 214305 (2006).
34. A. Werner and H. D. Hochheimer, Phys. Rev. B **25**, 5929 (1982).
35. B. P. Rai, Sol. Cell. **25**, 265 (1988).
36. A. R. Oganov, *High Pressure Crystallography*, Habilitation thesis, ETH Zurich (2007).
37. M. Hebbache and M. Zemzemi, Phys. Rev. B **70**, 224107 (2004).
38. O. L. Anderson, *Equations of State of Solids for Geophysics and Ceramic Science*, Oxford Univ. Press, Oxford (1995).
39. P. Vinet, J. H. Rose, J. Ferrante, and J. R. Smith, J. Phys.: Condens. Matter **1**, 1941 (1989).
40. A. Martinez-Ruiz, M. G. Moreno, and N. Takeuchi, Sol. St. Sci. **5**, 291 (2003).
41. W. Y. Ching, Y.-N. Xu, and K. W. Wong, Phys. Rev. B **40**, 7684 (1989).
42. P. W. Baumeister, Phys. Rev. **121**, 359 (1961).